Towards control of TiO thickness film in R-HiPIMS process with a coupled optical and electrical monitoring of plasma

D. Boivin, Aymane Najah, Ronny Jean-marie-desiree, Cédric Noël, Gérard Henrion, Stéphane Cuynet, Ludovic de Poucques

Surface & Coatings Technology 433 (2022) 128073

Contents lists available at ScienceDirect

Surface & Coatings Technology

journal homepage: www.elsevier.com/locate/surfcoat

Towards control of TiO_2 thickness film in R-HiPIMS process with a coupled optical and electrical monitoring of plasma

D. Boivin *, A. Najah, R. Jean-Marie-Désirée, C. Noël, G. Henrion, S. Cuynet, L. De Poucques

Université de Lorraine, CNRS, LJL, F-54000 Nancy, France

ARTICLE INFO

Keywords:
HiPIMS
Low pressure plasma
OES

ABSTRACT

In this work, optical emission spectroscopy and electrical measurements are implemented to investigate a reactive HiPIMS TiO_2 deposition process running at duty cycles lower than 16% and at a repetition rate of 1 kHz. Investigations focus on both the effect of the discharge pulse duration and the reactive gas (O_2) content in an Ar/O_2 gas mixture at fixed working pressures. It is shown that a competition occurs between the pulse duration and the target poisoning, the latter being favored with short pulse duration although the mean power is kept constant. An unusual hysteresis shape observed between the two sputtering modes is also discussed. From combined analyses of Ti emission line intensity, discharge current and deposited TiO_2 coating thickness, it is established that plasma diagnostics can be used effectively to control the deposition rate and to precisely manage the transition between metal and composite sputtering modes. Using these to calibrate a power feedback control loop could provide a better response compared to gas feedback control loop.

1. Introduction

Titanium oxide has many applications in various industrial fields, like optical and electronic devices [1,2], gas detection [3], water purification [4,5] or photovoltaic panels [6]. Titanium dioxide thin layers exhibit a wide range of interesting chemical and physical properties such as a high dielectric constant, high refraction index, good thermal and chemical stabilities, catalytic photo-activity [7] or biocompatibility and high hardness [8]. Thin layers of titanium oxide can be deposited by HiPIMS (high power impulse magnetron sputtering) [9–11], and conventional DC or RF magnetron sputtering [12].

HiPIMS [13–17] process is referred to as an ionized physical vapor deposition (IPVD) [18,19] one. In HiPIMS, a high ionization degree of the sputtered atoms can be achieved. Due to high applied voltage in HiPIMS, the pulse power is about one hundred times higher than in conventional magnetron sputtering while the cathode overheating can be avoided due to a rather low duty cycle. Consequently, the high ionization degree of the vapor phase allows conformal coatings to be deposited on complex-shape substrates by applying a bias voltage to the substrate [20]. The high ion bombardment of the substrate can also significantly influence the quality of coatings [21–23]. To deposit coatings like oxide, nitride, *etc*., HiPIMS can be operated in reactive mode (R-HiPIMS) with a reactive gas such as O_2 or N_2 mixed with the main non-reactive carrier gas, usually Ar. However, as in conventional MS (magnetron sputtering), the target poisoning by the reactive gas is also a concern in R-HiPIMS and the control of the R-HiPIMS process can become difficult. Poisoning of the target also changes the sputtering yield and the nature of the initial sputtered material into a compound material. Indeed, adding a reactive gas changes the discharge parameters such as voltage [24,25] and current [26]. Depending on the reactive gas amount in the gas mixture, the main experimental parameters (voltage or current) and the deposition rate exhibit a hysteresis that has been extensively studied [27,28]. For low $\%O_2$ in the gas mixture, the metallic sputtering mode allows achieving a high sputtering rate and non-stoichiometric coatings. For high $\%O_2$, the compound mode allows stoichiometric coatings to be deposited but at a low deposition rate. Between these two modes, the transition mode with a relatively high deposition rate and a stoichiometric composition of the coating is quite unstable. It is then necessary to find a reliable feedback control to make coatings within this transition mode.

Therefore, the coating industry needs a simple and reliable method to track the evolution of deposits over time. Extensive studies have been carried out to supply this need. They show that the process can be controlled by changing the pulse frequency [29–32]. Another method is to use a feedback control loop on the reactive gas flow [33,34], monitored with the intensity of an emission line (plasma emission

* Corresponding author.
E-mail address: dimitri.boivin@univ-lorraine.fr (D. Boivin).

https://doi.org/10.1016/j.surfcoat.2021.128073
Received 5 October 2021; Received in revised form 24 December 2021; Accepted 30 December 2021
Available online 6 January 2022

monitoring) [35–38] or a ratio between the intensity measured by OES (optical emission spectroscopy) and the current density [39]. One of the drawbacks of using a feedback control loop on the reactive gas flow is the response time delay necessary to stabilize the plasma state. Other authors control the deposition process by tuning the magnetic field strength surrounding the target [40,41]. Such a method is, however, not convenient to be implemented on industrial installations.

In this study, a method is proposed to enforce the feedback control loop on electrical parameters (as suggested in [29–32]) by coupling electrical measurements with optical emission spectroscopy.

This study aims to highlight the correlation between OES and integrated current measurements with the thickness of deposits in Ar/O_2 mixture. These correlations are investigated for two series of experiments. The first one consisted in varying the oxygen content in the gas mixture; the second one dealt with the effect of high voltage pulse width. The study also focuses on the characterization of the hysteresis phenomenon as a function of the high voltage pulse width for very low percentages of oxygen in the gas mixture at constant working pressure.

2. Experimental setup

The plasma reactor consists of a cylindrical stainless-steel chamber of 30 cm in diameter and 35 cm in height. A circular planar balanced magnetron cathode, with the magnetic characteristic shown Fig. 1, is set in the chamber.

A 2″ diameter pure titanium (99.99%) target with a thickness of 3 mm is used. The substrate is located at 5 cm from the target surface on a grounded substrate holder. Prior to deposition, the chamber atmosphere is evacuated by a primary pump (ACP 15 Adixen) and a turbomolecular pump (ATP 400 Adixen) down to a residual pressure of 1.2×10^{-4} Pa. An AHC 2010 Adixen gauge measures the pressure inside the chamber. The combined gauge used was calibrated by a capacitive gauge. Then different positions of the throttle valve have been determined to get the desired working pressures. These positions were tested up to 10% O_2; no pressure variation was observed. Ar and O_2 gas flows are injected into the chamber at 15 cm from the target center and parallel to the target surface. The total gas flow (Ar and O_2) is set to a constant value of 19 sccm (standard cubic centimeter per minute) with two mass flowmeters of 20 sccm full scale. This is achieved by decreasing the Ar gas flow when the O_2 one is increased. For a better accuracy at small percentages of oxygen, a 3 sccm flowmeter is used and the total flow is kept at 19 sccm. A constant total working pressure of 0.7 Pa is set by a throttle valve. In order to maximize measurement accuracy and only for the hysteresis study, the total working pressure is fixed at 1.4 Pa and only the 3 sccm flowmeter is used to finely control the % O_2 in the gas mixture. The % O_2 refers to the percentage of the O_2 injected gas flow by the total gas flow.

The target is connected to a high voltage pulse generator (MELEC SIPP 2000), also able to work in direct current regime (DC). The high voltage pulse waveform is driven by an arbitrary function generator (Tektronix AFG 3022C dual channel). The mean power $<P>_T$ (Eq. (1)) during the HiPIMS period T and the voltage pulse frequency are set at ≈ 45 W and 1 kHz, respectively.

Consequently, the mean power during the plasma $<P>_{Td}$ (Eq. (2)) depends on the discharge duration T_d (the pulse width setting), as presented in Fig. 2. To support this, the power pulse evolution calculated from the current and voltage measurements for various pulse widths is shown Fig. 2. In the present study, the pulse width varies from 10 μs to 160 μs, corresponding to a duty cycle in the range 1 to 16%.

$$< \mathrm{P} >_{\mathrm{T}} = \frac{1}{T}\int_0^T P(t)dt \tag{1}$$

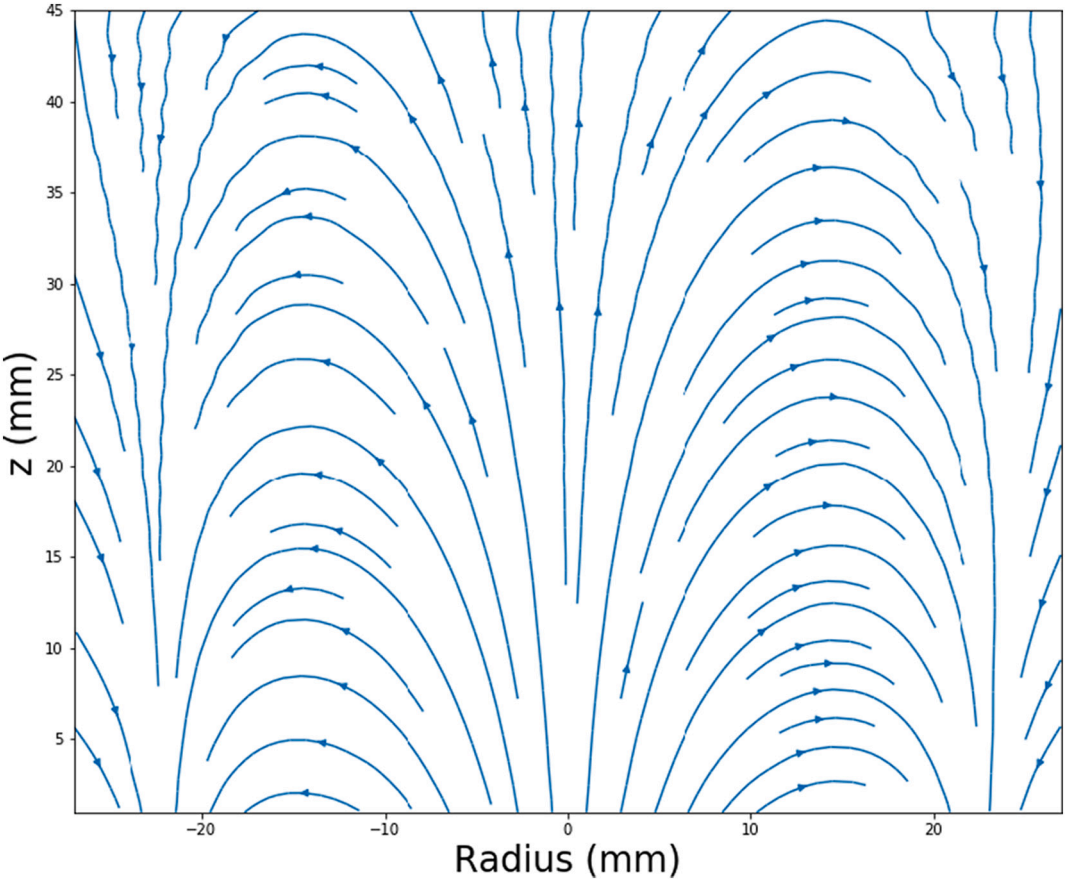

Fig. 1. Magnetic characteristic of the magnetron (radius = 0 corresponds to the center of the target).

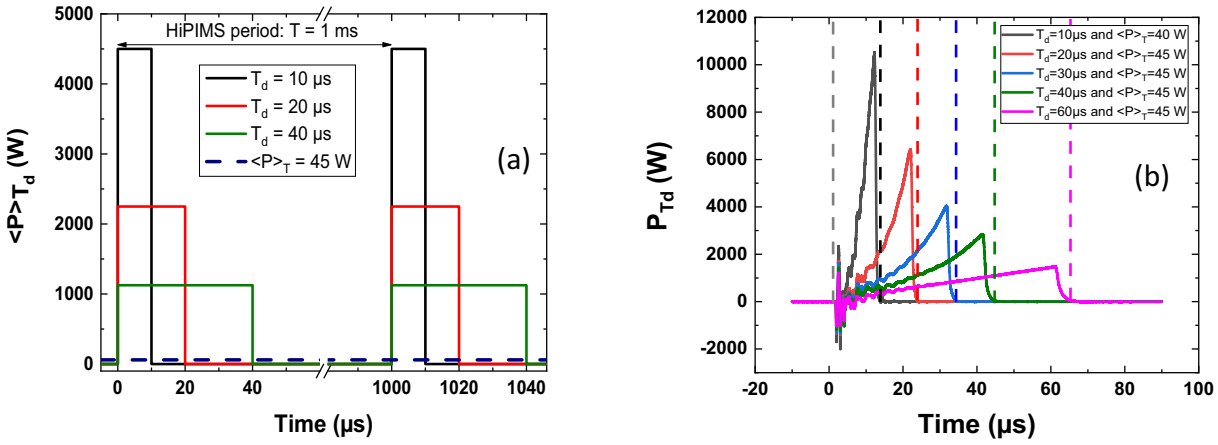

Fig. 2. (a) Schematic diagram of the mean pulse power $<P>_{Td}$ for various HiPIMS discharge durations (T_d) and at a fixed mean power $<P>_T$ for a HiPIMS period $T =$ 1 ms. (b) Power pulse for various pulse width. The pressure and the % O_2 in the gas mixture are fixed at 0.7 Pa and 2% respectively. HiPIMS period of 1 ms and a mean power of 45 W. For the 10 µs short pulses, the HiPIMS generator becomes not able to reliably keep the 45 W setpoint.

$$< P>_{Td} = \frac{1}{T_d}\int_0^{T_d} P(t)dt \tag{2}$$

A voltage probe (CalTest Electronics CT4028 with a bandwidth from DC to 220 MHz) and a current probe (MagneLab CT1.0-B, bandwidth up to 500 MHz) are used to measure the voltage-current characteristics of the discharge. These two probes are connected to an oscilloscope (Lecroy Wave runner 104Xi 1GHz). OES measurements are performed with a Jobin Yvon TRIAX 550 spectrometer equipped with a 1800 gr.mm^{-1} grating and an intensified charged couple device camera (ICCD). The light emitted by the plasma is collected *via* a collimator located inside the reactor and through a quartz window. The collimator (1 cm in diameter, 9 cm in length) is used to limit the observation area. The axis of the collimator is positioned parallel to the target surface at a distance z = 1 cm. An optical fiber is placed outside of the chamber and is aligned with the axis of the collimator, behind a quartz lens used to focus the light emitted by the plasma on the optical fiber aperture. The spectral resolution of the spectrometer is 0.07 nm with an entrance slit width set to 50 µm. The experimental setup for the OES measurements is shown in Fig. 3.

The plasma emission signal was acquired by OES, the exposure time of the camera is set to 100 ms. Then an acquisition corresponds to 100 discharges. Spectra are averaged 20 times. This time-averaged optical emission spectroscopy measurements (TA-OES) were carried out for different plasma conditions within two sets of experiments as reported in Table 1.

Thin films were deposited on flat crystalline (100) silicon wafers. The deposition time was fixed to 4 h regardless the magnetron sputtering conditions. Prior to deposition, Si substrates were washed in an ultrasonic bath in acetone for 10 min and then in ethanol for 10 min. The clean silicon wafer was then hooked to the grounded substrate-holder by a polyimide Kapton film. After HiPIMS deposition, removing the Kapton film allows measuring the thickness of the formed thin film by

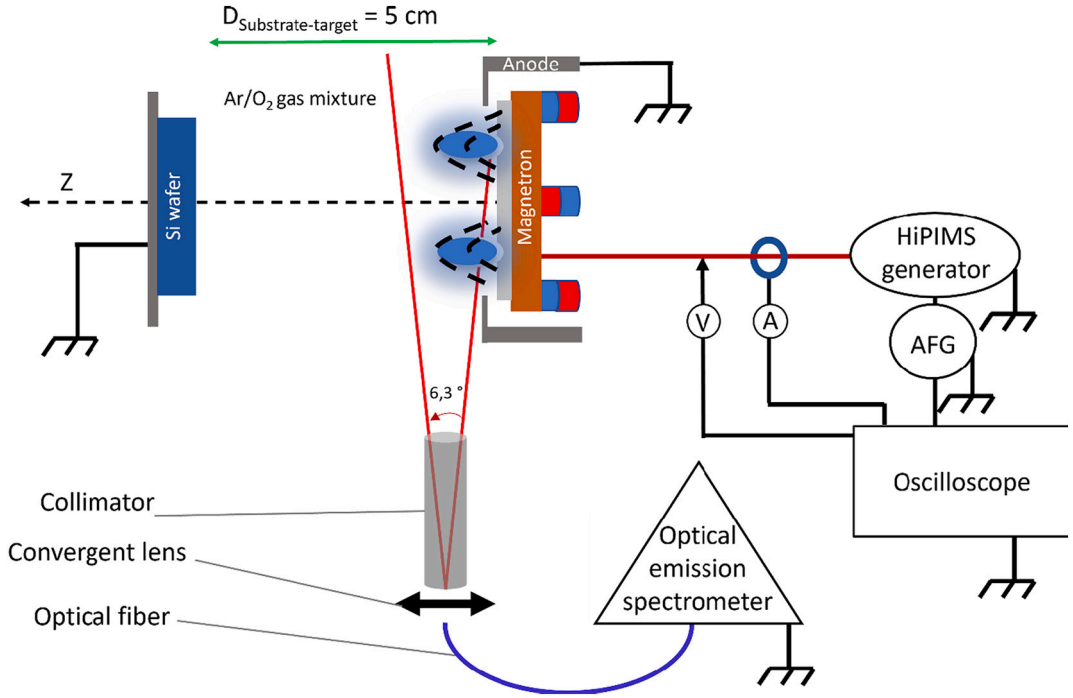

Fig. 3. Experimental scheme for OES measurements (AFG stands for Arbitrary Function Generator).

Table 1
Experimental conditions for the two sets of deposition conditions in Ar/O_2 gas mixtures.

	P (Pa)	T (ms)	O_2 (%)	Pulse duration T_d (μs)	$<P>_T$ (W)	$<P>_{Td}$ (W)
Set 1	0.7	1	0 to 5	20	45	1970
Set 2	0.7	1	2	10 to 60	39 to 47	3260 to 747

profilometry (step height measurement). The profilometer is a Bruker Dektak XT touch profilometer with a diamond tip of 2 μm radius. The thickness values measured by profilometry were compared to scanning electron microscopy (SEM Gemini Zeiss) observations of sample cross sections.

3. Results

Fig. 4 presents an OES spectrum of the HiPIMS plasma. Several emission lines from titanium atoms and titanium ions are clearly identified. Only the most intense lines are indexed in Fig. 4. In the present study, the Ti intensity at 365.35 nm and the Ti^+ one at 368.52 nm are used. Regarding the Ti^+ line, it corresponds actually to a doublet line issued from two levels with the same electronic configuration, except for the spin values. It is therefore reasonable to consider that both levels are populated through similar mechanisms.

The emission intensity of a given line can be written:

$$I_{ij} = C(\lambda_{ij})\, A_{ij}[M_i]\, h\nu_{ij} \tag{3}$$

where subscripts i, j refer to the upper and lower level of the transition, respectively. A_{ij} is the Einstein's coefficient of spontaneous emission, $[M_i]$ is the population density of the upper state of species M, $C(\lambda_{ij})$ is a constant including the observed plasma volume and the spectral response of the optical system at the wavelength λ_{ij}, ν_{ij} is the frequency of the transition and h the Planck's constant.

OES measurements allow determining only the excited state density $[M_i]$ of species M. However, ground states of atoms are by far much more populated than excited states and are the main species that contribute to the coating deposition. In order to correlate the measured OES intensities with the coating growth rate, a relation between $[M_i]$ and the density of ground state $[M]$ is therefore required.

For this, several production and loss mechanisms can be involved in the population of the excited state M_i. The main processes are:

Electron collision with the ground state

$$M + e^- \rightarrow M_i + e^- \tag{4}$$

Electron-ion recombination

$$M^+ + e^- \ (+ a\ third\ body/species) \rightarrow M_i \tag{5}$$

Radiative cascade from higher energy levels

$$M + e^- \rightarrow M_{k>i} \rightarrow M_i + h\nu_{ki} \tag{6}$$

Radiative decay

$$M_i \rightarrow M_{l<i} + h\nu_{il} \tag{7}$$

Collision with another heavy species Y (quenching)

$$M_i + Y \rightarrow M_{l<i} + Y^* \tag{8}$$

At a very low pressure of 0.7 Pa, electron-ion recombination and quenching are very unlikely. Moreover, the probability of populating a higher energy than i, starting from the fundamental state as described by reaction (6), is low (Maxwell–Boltzmann statistics) and leads us to neglect this reaction. With these assumptions, it is reasonable to consider only reactions (4) and (7) as the dominant mechanisms involved in the population of M_i.

Consequently, Eq. (3) becomes:

$$I_{ij} = C(\lambda_{ij}) n_e [M] k^i_{eM} \frac{A_{ij}}{A_i} h\nu_{ij} \left(A_i = \sum_{l<i} A_{il} \right) \tag{9}$$

n_e being the electron density, A_i is the inverse of the radiative lifetime of the excited state i, k^i_{eM} the reaction coefficient of process (4) and $[M]$ the density of titanium species at the ground state. In Eq. (9), k^i_{eM} depends on the electron energy distribution function during the HiPIMS discharge. Similarly, the discharge current, or the current density j given by $j = n_e q <v_e>$ where q is the electron charge, n_e and $<v_e>$ the electron density and average velocity respectively, also depends on both the electron density (n_e) and the electron velocity distribution function. Moreover, the discharge current integrated over the current pulse is:

$$I_{int} = \int_0^{T_{int}} I(t)dt \tag{10}$$

where T_{int} is the duration of the current pulse, *i.e.* the pulse width (T_d) plus the fall-time of the current (see Fig. 5).

Therefore, dividing the emission line intensity (Eq. (9)) by the integrated current (Eq. (10)) leads us to obtain the *TA_OES signal*/I_{int} ratio, which allows eliminating the effect of any variation of the electron population. Based on these assumptions, the *TA_OES signal*/I_{int} ratio can be compared with the film thickness to investigate the correlation between Ti-species optical emission contribution and the coating growth.

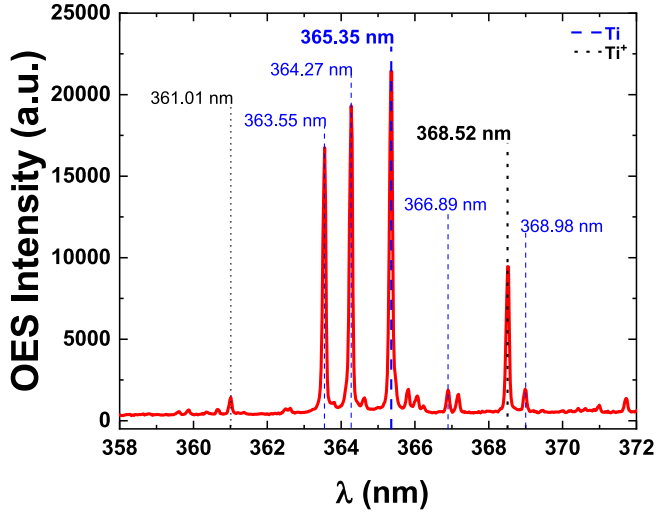

Fig. 4. Typical part OES Spectrum used to monitor the emission line intensity of neutral titanium (Ti) and titanium ion (Ti^+). In pure Ar, 20 μs 0.7 Pa $<P>_T$ 45 W with a slit of 100 μm.

3.1. Impact of O_2 in the gas mixture on OES and thickness measurements

The influence of O_2 content in the gas mixture was studied at a fixed discharge duration (T_d = *20* μs; set 1 in Table 1). The corresponding discharge voltage and current are shown in Fig. 5. Regardless the composition of the gas mixture (metallic mode ($[O_2]$ = *0%*); oxidized mode ($[O_2] \geq$ *1%*)) and for both voltage and current measurements, a stable and dampened oscillation occurs at the voltage rising (at t_0, as defined in Fig. 5) due to the transient regime. Beyond *10* μs after t_0, the dampened oscillations decrease enough and electrical values measurements can be easily exploited (see inset in Fig. 5). Firstly, one can observe an increase of the absolute voltage value from about 480 to 510 V, between 10 and 12 μs, as soon as 1%O_2 is added to the argon gas. Since the mean power $<P>_T$ is set at 45 W, this voltage increase occurs to compensate the decrease of the mean current over T_d from 4.3 A to 3.9

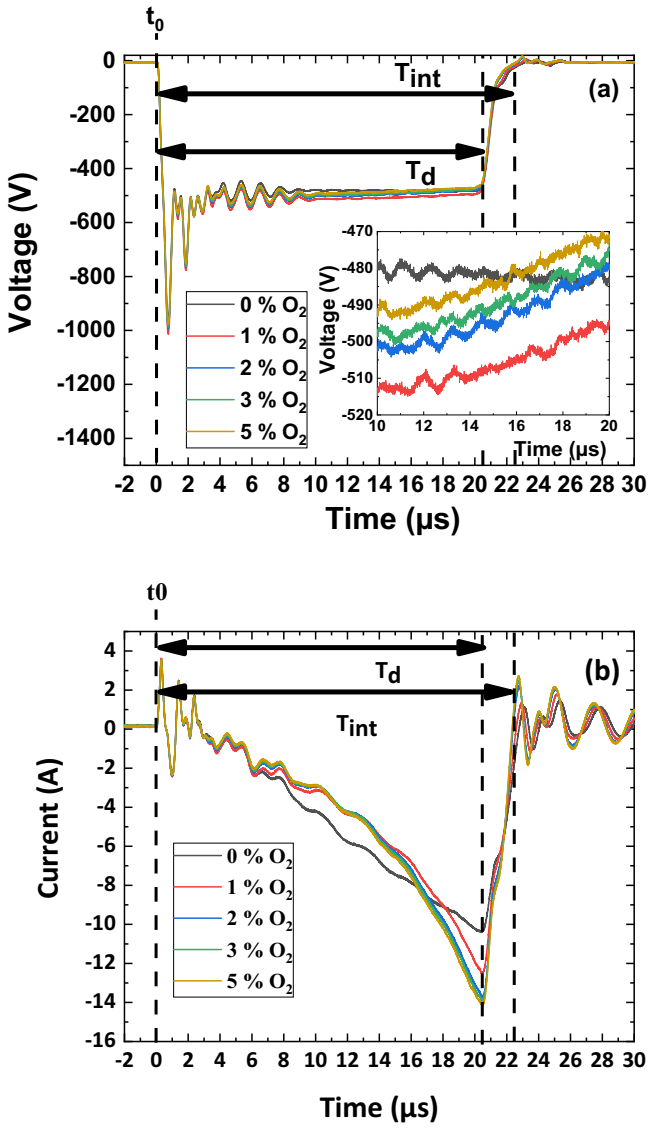

Fig. 5. Discharge voltage (a), current (b) as a function of the percentage of O_2 in the gas mixture for a pulse width of 20 µs and a voltage pulse period of 1 ms. The pressure is 0.7 Pa and the mean power $<P>_T$ is set at 45 W.

A for metallic and oxidized (1% O_2) modes, respectively. When O_2 content in the gas mixture is further increased beyond 1%, the voltage value starts to slightly decrease and the associated $<I>_{Td}$ increases consequently to keep the fixed $<P>_T$. Secondly, the shape of the voltage curves displayed in the inset of the Fig. 4a differ from each other. As soon as the oxidized mode is reached ($\geq$ 1% O_2), the shape of the current pulses remains quite unchanged, irrespective of the O_2 content. In metallic mode the voltage exhibits a plateau starting at t_0 +10 µs and until the end of T_d while in oxidized mode the voltage measurements decrease by about 3% quasi-linearly over the same time range. According to Gudmundsson et al. [42] in metallic mode, the time variation of the current over one current pulse is due to the ionization of the argon gas followed by the progressive addition of a part of the sputtered and ionized titanium atoms. As for Ar^+, Ti^+ ions are accelerated back to the target and contribute to the current.

Aiempanakit et al. [26] studied the R-HiPIMS process with oxygen and a Ti target. In oxidized mode, they indicated that the initial increase of the current during the first microseconds is due to Ar^+ ions. As soon as the sputtered oxygen atoms from the poisoned target are ionized in the plasma, a part of these ions is back attracted. By impinging upon the target, the latter contribute to a large ionic current at the end of the HiPIMS pulse. They concluded that Ti ions less contribute to the current in oxidized mode than in metallic mode since titanium is less sputtered when the target is oxidized. These hypothesis and previous results seem to be consistent with the measured discharge currents shown in Fig. 4(b) since no significant current evolution can be observed beyond 2% O_2. Consequently, in oxidized regime, the target current seems mainly driven by the oxidation state of the target surface and not by the amount of O_2 in the plasma volume, under the present conditions (up to 5% O_2). Based on these first electrical measurements during the HiPIMS deposits, the target surface seems to reach a stable state whatever the gas mixture changes beyond 2% O_2 in the present conditions. This should then have a major impact on R-HiPIMS deposits.

The comparison between the TiO_2 coating thickness obtained after 4 h of sputtering and the *TA-OES signal/I_{int}* ratio for titanium species is shown in Fig. 6. It is worth noting that, as the emission lines of the titanium atoms and ions evolve in the same way as a function of the % O_2, we have chosen the most intense titanium atom line (at 365.35 nm) for the HiPIMS process control method proposed in this work. One can observe in Fig. 6 that both quantities sharply decrease as soon as 1% O_2 is added in the gas mixture. This decrease is undoubtedly due to the poisoning of the target by oxygen, which is in good agreement with the measured discharge currents and the above-mentioned hypothesis. Indeed, the reactivity between titanium and oxygen unavoidably results in the formation of a compound layer on the target. In R-HiPIMS regime, the bombardment of the target by oxygen ions during the discharge and the adsorption of neutral O atoms and O_2 molecules on the target during both the discharge and the temporal post-discharge are the main processes involved in the target poisoning. Since the Ti—O covalent bond is much stronger than the Ti—Ti metallic one, the sputtering yield drastically decreases [26] from the metallic mode in pure Ar to the oxidized mode at 1% O_2. Therefore, it seems that in the present conditions of HiPIMS, as soon as 1% O_2 is present in the gas mixture, a discharge duration of 20 µs is not long enough to sputter efficiently the growing oxide layer formed at the target surface, especially on the racetrack surface.

Furthermore, as seen in Fig. 6 the coating thickness and the *TA_OES signal/I_{int}* evolve in the same way. El Farsy et al. [43] observed a similar behavior in the case of a titanium target in Ar/N_2 gas mixture. During their study, they used time-resolved tunable diode laser induced fluorescence analysis (TR-TDLIF) to determine the flux of the ground state neutral titanium atoms. By adding 1% N_2, a drastic decrease in both the titanium atoms flux and the thin film thickness was observed. This effect

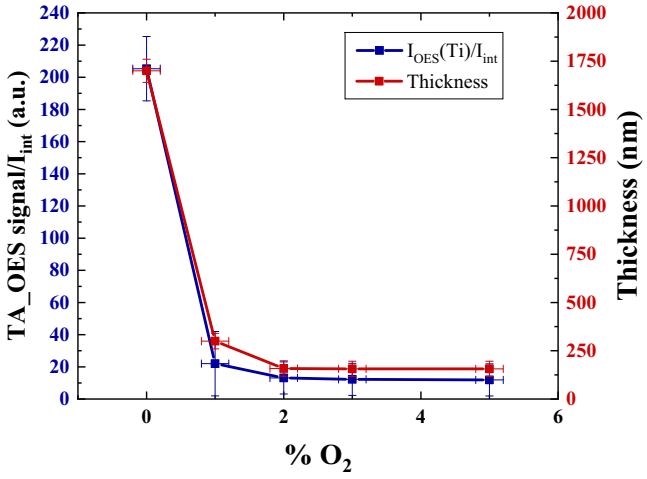

Fig. 6. Variation of the layer thickness (right axis) and TA_OES signal/I_{int} ratio (left axis) as a function of the percentage of O_2 with T_d = 20 µs. The pressure is 0.7 Pa, the duration of the deposits is 4 h and the mean power $<P>_T$ = 45 W.

was attributed to the target poisoning during the relatively long post-discharge (~ 1 ms) and the chosen short discharge duration (10 μs). According to these authors, a 10 μs power pulse seems to be not long enough to sputter efficiently the compound layer at the extreme surface of the racetrack. By comparing the neutral titanium flux with the thickness, they obtained the same trend of both quantities with the percentage of nitrogen in the gas mixture. In the present work, the *TA-OES signal/I_{int}* ratio presented above seems to well reflect the density of titanium species that contribute to the deposits. Moreover, beyond 2% O_2, the *TA-OES signal/I_{int}* ratio and the film thickness do not vary. This is in good agreement with the current measurements and seems to support the previous hypothesis, *i.e.* the target surface state does not change over 2% O_2.

One can note that it is possible to establish a proportionality factor between the *TA_OES signal/I_{int}* ratio and the obtained thickness of the deposited layer. A similar factor should be valid for other experimental setup albeit subject to take into account each specific element of the HiPIMS process (reactor geometry, magnetron cathode, OES detection system, electrical probes, *etc.*). It could however be easily calibrated. In the present case the proportionality factor is found to be about 9.

3.2. Influence of the discharge duration at 2% O_2 in the gas mixture

The *TA_OES signal/I_{int}* ratio seems to be a good monitoring parameter of the HiPIMS process as soon as the discharge duration is set. As the applied power is concentrated during the pulse width, this section deals with the influence of the latter while the oxygen gas content in argon is set at a constant value of 2% that corresponds to the sputtering regime in the oxidized mode at $T_d = 20$ μs. As mentioned above (Fig. 1), keeping the HiPIMS mean power at a constant value ($<P>_T = 45$ W) implies that the mean pulse power $<P>_{Td}$ decreases when the pulse width T_d increases. The values associated with the pulse width are given in Table 2.

Despite the set point at $<P>_T = 45$ W, it should be noticed that for short pulse duration ($T_d < 20$ μs), the mean power does not reach the requested value. This is due to the power generator that reaches its limits in terms of real-time regulation for such short pulse width.

Therefore, two data sets were collected, one for T_d in the range 10 to 20 μs and the second one for T_d ranging from 20 to 60 μs. Furthermore, the two data sets were separated by a few days period during which other experiments were carried out in the HiPIMS reactor. Consequently, the reactor conditions have obviously evolved (*e.g.* the target erosion state, wall state, *etc.*).

Fig. 7 represents the variation of *TA_OES signal/I_{int}* ratio and the layer thickness as a function of the discharge duration, at 2% O_2 and working pressure of 0.7 Pa. It shows that both *TA_OES signal/I_{int}* and coating thickness, significantly increase with the pulse width. Since this variation is more than a factor 2, it cannot be explained by the slight increase of I_{int} and $<P>_T$ (or P_{int}) over the pulse width (10–20%). In addition, quasi-constant values of *TA_OES signal/I_{int}* and of thickness could have been expected, due to the compensation of the pulse duration by the pulse power during the discharge ($<P>_{Tint}$ calculated with Eq. (11)) in order to maintain the mean power $<P>_T$ close to 45 W. Initially, the quantity of sputtered atoms was expected to be comparable.

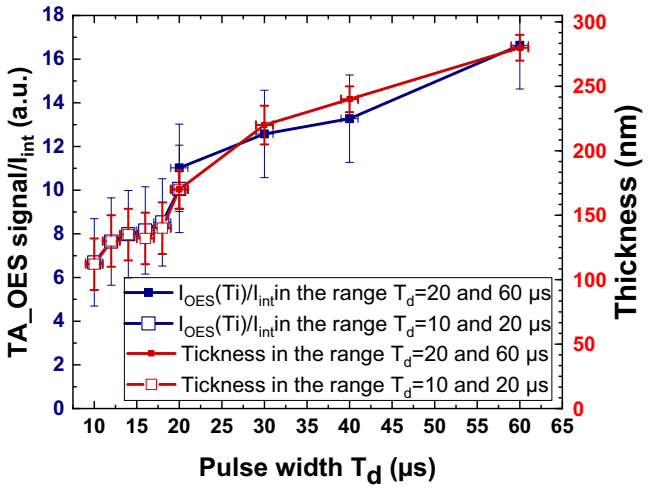

Fig. 7. Correlation between the coating thickness and the time averaged OES intensity divided by the integrated current. The pressure is 0.7 Pa, the deposition time is 4 h, the HiPIMS period is 1 ms, 2% O_2 in the Ar/O_2 gas mixture and the mean powers are indicated in Table 2.

$$\langle P \rangle_{T_{int}} = \frac{1}{T_{int}} \int_0^{T_{int}} P(t)dt \tag{11}$$

Under our conditions, even if the product $<P>_{Tint} \times T_{int} = P_{int}$ increases by a factor of ~1.2, the thickness increases by a factor of 2.5. Then this increase in power does not seems enough to explain the increase of the thickness. This effect is more likely due to a more efficient sputtering of the target. The pulse width turns out to be the dominant parameter in our conditions while the plasma power ($<P>_{Tint}$) seems to have a limited impact. Even if $<P>_{Tint}$ is decreased, increasing the pulse width can likely favor the sputtering of the oxide superficial layer that has grown in between two successive power pulses, leading to a more efficient sputtering of titanium.

In all our conditions, since the *TA_OES signal/I_{int}* ratio is in good agreement with the coating thickness, it would seem to reflect the evolution of the sputtered titanium atoms density. It is therefore possible to follow the evolution of the HiPIMS process by coupling OES and current measurements according to the pulse width.

3.3. Study of the influence of the pulse width on the hysteresis phenomenon at 1.4 Pa

As seen in Section 3.2, pulse width T_d could be the dominant parameter to obtain an efficient sputtering of the target in oxidized mode and at almost constant mean power $<P>_T$. In order to support the latter, the hysteresis phenomenon has been studied for different values of T_d. As seen in Fig. 6, as soon as 1%O_2 is added to the gas mixture, the *TA-OES signal/I_{int}* ratio and the growth rate strongly decrease, depicting

Table 2
Values of current, voltage and power associated with pulse width ranging between 10 and 60 μs. The pressure is 0.7 Pa, with 2%O_2 in the Ar/O_2 gas mixture.

	First set of measurements						Second set of measurements			
T_d (μs)	10	12	14	16	18	20	20	30	40	60
T_{int} (μs)	12	14	16	18	20	22	22	32	42	62
$<U>_{Tint}$ (V)	545	530	510	500	490	485	460	440	430	430
$<I>_{Tint}$ (A)	7	6.4	5.3	4.9	4.7	4.2	4.3	2.9	2.2	1.5
$<P>_{Tint}$ (kW)	3.1	2.8	2.5	2.3	2.2	2.0	1.9	1.3	1.0	0.7
I_{int} (A.μs)	88	92	97	99	101	102	100	100	101	103
P_{int} (mJ)	39.0	39.6	41.2	42.0	42.8	43.1	45.3	45.4	45.6	46.5
$<P>_T$ (W)	39	40	41	42	43	43	45	45	46	47

the transition from a metallic to an oxidized sputtering mode. Henceforth a hysteresis phenomenon should occur below 1% O_2 for $T_d = 20$ µs [28]. In order to characterize the hysteresis phenomenon and investigate the influence of the pulse width on this hysteresis, measurements with oxygen percentages lower than 1% were carried out with an appropriate O_2 flowmeter.

Fig. 8 shows the evolution of *TA_OES signal/I_{int}* as a function of the % O_2 in HiPIMS regime for different pulse widths (10–160 µs). A comparison with the DC regime (45 W) is also proposed. An hysteresis can be observed for a %O_2 lower than 2%, whatever is the HiPIMS pulse width. Three different regimes can be identified on each hysteresis when increasing the O_2% (black curves) and decreasing it (red curves). Fig. 8d well represents these regimes. With T_d = 80 µs, the target starts to be sputtered in the metallic regime for %O_2 ranging from 0 to 0.5% and the *TA-OES signal/I_{int}* value is then the highest. From 0.5% to 0.9% O_2, the *TA-OES signal/I_{int}* ratio strongly decreases, and a "plateau" is reached up to 1.2% O_2. This regime between 0.9% and 1.2% O_2 can be interpreted as an "intermediate mode". For %O_2 greater than 1.2%, a new transition takes place, and the fully oxidized mode is then reached with a lowest value of the *TA-OES signal/I_{int}* ratio. Nevertheless, for the shorter pulse widths, T_d = 10 µs (Fig. 8a) and T_d = 20 µs (Fig. 8b), the transition between the metallic mode and the intermediate mode seems occurring

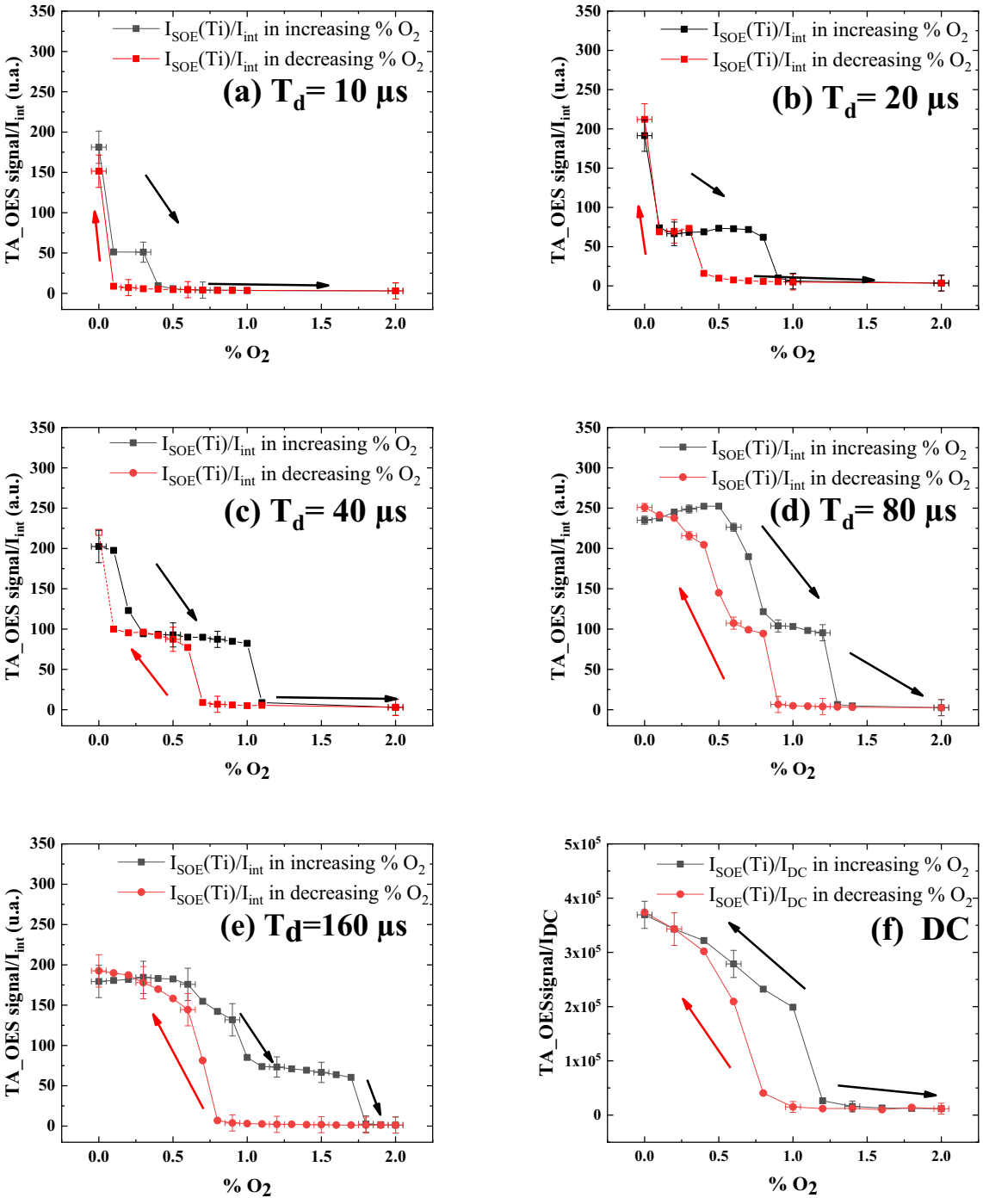

Fig. 8. Hysteresis for different pulse widths in function of O_2 percentages. (a) 10 µs, $<P>_T$ = 46 W; (b) 20 µs, $<P>_T$ = 49 W (c) 40 µs; $<P>_T$ = 51 W (d) 80 µs, $<P>_T$ = 49 W; (e) 160 µs, $<P>_T$ = 47 W and (f) DC, P = 45 W. The pressure is 1.4 Pa and the HiPIMS period is 1 ms.

immediately as soon as oxygen is introduced in the gas mixture (0.1% O_2). By increasing the % O_2 in the gas mixture, the transition from the intermediate mode to the oxidized mode occurs at lower % O_2 values than for $T_d = 80$ μs: between 0.3% O_2 and 0.5% O_2 for $T_d = 10$ μs, and between 0.8% O_2 and 1% O_2, for $T_d = 20$ μs. Fig. 8c shows that the sputtering metallic regime starts to persist with the increase of % O_2 only when T_d is equal to or greater than 40 μs. This indicates that a T_d value lower than 40 μs, in the present conditions, is not long enough to remove the oxide thin film formed at the target surface between each pulse once 0.1% O_2 is present in the gas mixture. For $T_d = 160$ μs (Fig. 8e), it should also be noted that the transition from metallic mode to intermediate mode occurs between 0.5% O_2 and 1.1% O_2; the transition from intermediate to compound mode takes place between 1.7% O_2 and 1.8% O_2, making it the largest intermediate mode range in terms of %O_2. This could help for an easier control of the deposition process in such conditions. Decreasing the %O_2 in the gas mixture (red curves in Fig. 8) makes the transitions from oxidized mode to metallic one to occur for different %O_2 ranges, namely from 0.1% to 0% for $T_d = 10$ μs (Fig. 8a), from 0.4% to 0% for $T_d = 20$ μs (Fig. 8b), from 0.7% to 0.1% for $T_d = 40$ μs (Fig. 8c), from 0.9% to 0.3% for $T_d = 80$ μs (Fig. 8d), and from 0.8% to 0.3% for $T_d = 160$ μs (Fig. 8e). Globally and regardless the pulse width value, the return to a metallic mode from an oxidized one needs to reduce more significantly the amount of oxygen in the gas mixture. To get the preceding example with $T_d = 80$ μs, the beginning of the oxidized mode for the increasing part of the hysteresis is at 1.4% O_2 while for the decreasing part, the end of the oxidized mode is at 0.9% O_2. This could be attributed to the different sputtering yields between the metallic mode and the oxidized one [26].

The intermediate mode is not observed in DC magnetron sputtering (Fig. 8f). To understand the origin of this mode, the *TA-OES signal* of other species and the integrated current I_{int} were measured. Fig. 9 presents the *TA-OES signal*/I_{int} values of Ti^+ ions at 368.52 nm (Fig. 9a), the pulse integrated current I_{int} (Fig. 9b), *TA-OES signal*/I_{int} values of O atoms at 777.19 nm (Fig. 9c) and *TA-OES signal*/I_{int} values of Ar atoms at 751.47 nm (Fig. 9d). The intermediate mode is visible on the titanium ion but neither on the current discharge nor on oxygen and argon lines. Henceforth it seems that this intermediate mode is more likely related to a surface state of the target than to the properties of the plasma. Indeed, G. S. Chen et al. [43] reported similar results by studying TiO_2 deposition in RF magnetron sputtering. They showed that by adding a little amount of oxygen in the gas mixture, the intensity of titanium emission lines decreased. Using XRD analysis of TiO_2 coatings grown with different O_2 contents, they pointed out the presence of different crystalline phases resulting from various degrees of oxidation of the titanium target. However, during their investigations, they did not observe such intermediate mode. This change in surface state of the target as reported by Chen et al. [44] could explain our results. Another hypothesis could relate to the effect of the back attracting of titanium ions towards the target, which is important in HiPIMS process. Indeed, the deposition of Ti ions on the target could favor the consumption of oxygen during the discharge. It would highlight that more and more O_2 is required to reach the third mode in HiPIMS, *i.e.* the oxidized mode. The intermediate mode could therefore be considered as a dynamic equilibrium state, where the consumption rate of the oxygen and the sputtering rate of the target are comparable. Nevertheless, it is not possible to draw a definitive conclusion about the origin of this intermediate mode.

Comparing the hysteresis given by the different pulse widths (Fig. 8), the shorter the pulse width, the lower the O_2 content required to oxidize

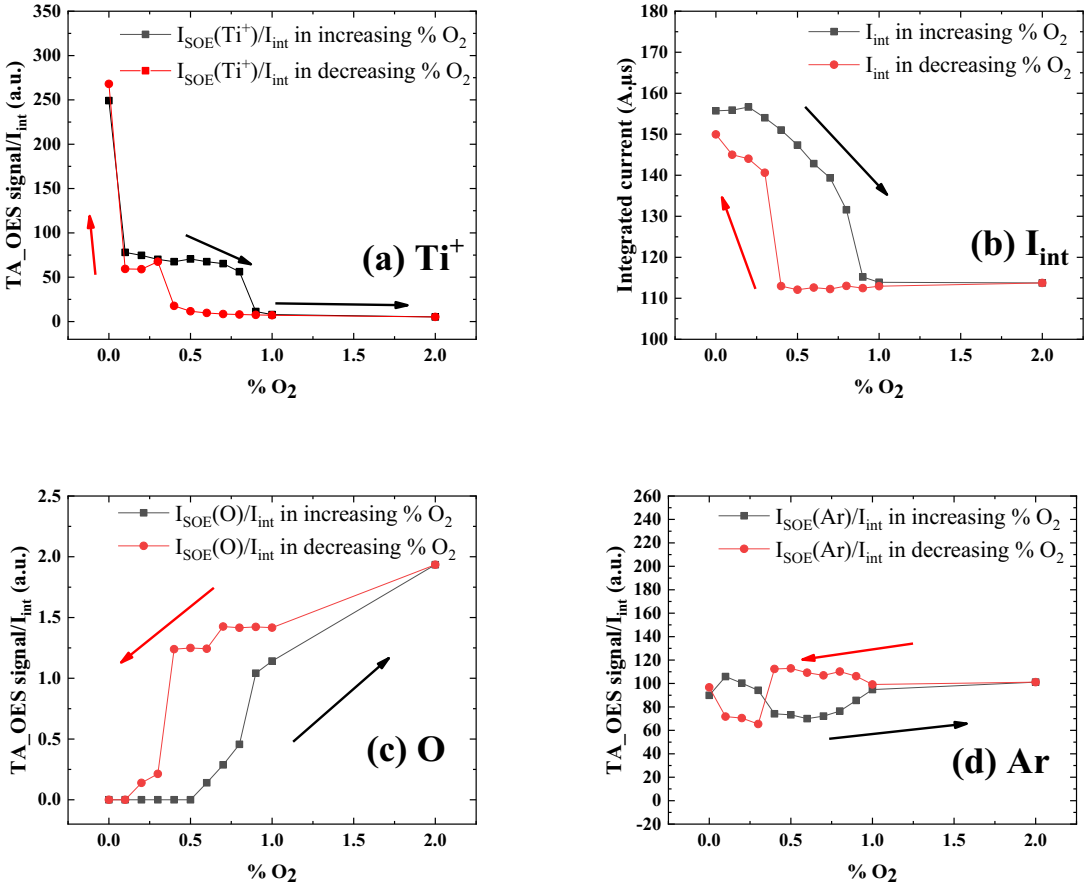

Fig. 9. Hysteresis for different quantities: (a) TA_OES signal/I_{int} ratio of titanium ion; (b) integrated current; (c) TA_OES signal/I_{int} ratio of Oxygen and (d) TA_OES signal/I_{int} ratio of argon. Pressure = 1.4 Pa and pulse width = 20 μs. The HiPIMS period is 1 ms and $<P>_T$ = 49 W.

the target. Increasing the pulse width can likely favor the sputtering of the oxide superficial layer (grown in between two successive power pulses), in competition with its formation. This result supports hypothesis that pulse width seems to be the most influent parameter on the Ti-atoms production under the present conditions, as discussed in Section 3.2.

.

4. Conclusion

This work is mainly devoted to the development of a reliable tool devised to control thin layer thickness in R-HiPIMS deposition process. For this purpose, time-average OES (TA-OES) and thickness measurements were performed to characterize TiO_2 HiPIMS deposition process as a function of both the oxygen content in Ar/O_2 gas mixture and the width of the power pulse T_d (or T_{int}). At fixed discharge duration of 20 μs and mean pulse power $<P>_{Tint}$ of about 2 kW, with a change from 0 to 1% O_2 in the gas mixture in a single step, the hysteresis phenomenon is not visible. Once 1% O_2 in the argon gas is reached, a huge decrease of the film thickness is observed, which is attributed to the reactivity between titanium target surface and oxygen. Another study, at 2% O_2 and a total mean power during one HiPIMS period fixed (~ 45 W) was carried out in order to obtain a quantity of sputtered atoms expected to be comparable. The thickness increases by a factor of 2.5 when the pulse width is increased from 10 to 60 μs. This effect could be attributed to the difficulty of sputtering an oxidized titanium target at shorter pulse width, even if the mean pulse power $<P>_{Tint}$ is higher. Therefore, regarding the sputtering efficiency, the pulse width turns out to be the dominant parameter in our conditions while the plasma power seems to have a very limited impact. This behavior has been supported by hysteresis phenomenon measurements at very low percentages of oxygen (% O_2 < 2%). Indeed, in the latter condition, a longer pulse width induces a shift of the hysteresis towards the higher O_2 percentages. This trend reflects a better sputtering efficiency at short pulse width, since a higher O_2 content is required to oxidize the target surface.

In all our conditions, the ratio between the TA-OES signal of titanium atoms and the integrated discharge current ($TA\_OES\ signal/I_{int}$) seems to be in good agreement with the thickness. Thus, it seems that this ratio well reflects the titanium species density which contributes to the deposits. Following the evolution of the HiPIMS process by means of OES coupled with current measurements under our plasma conditions proves to be reasonable. A method based on the evolution of the $TA\_OES\ signal/I_{int}$ ratio could greatly simplify both the monitoring and the control of industrial scale deposition processes, once adapted to the reactor geometry. Compared to feedback control on the gas flow, using the $TA\_OES\ signal/I_{int}$ ratio to monitor the injected power can provide an instantaneous response of the deposition process, *e.g.* to obtain a constant thickness.

CRediT authorship contribution statement

D. Boivin: Formal analysis, Conceptualization, Writing – review & editing, Writing – original draft, Data curation, Investigation. **A. Najah:** Writing – review & editing. **R. Jean-Marie-Désirée:** Writing – review & editing. **C. Noël:** Supervision, Validation, Resources. **G. Henrion:** Supervision, Validation. **S. Cuynet:** Supervision, Validation, Resources. **L. De Poucques:** Supervision, Validation, Resources.

Declaration of competing interest

The authors declare that they have no known competing financial interests or personal relationships that could have appeared to influence the work reported in this paper.

Acknowledgments

This work was supported by the European Regional Development Fund through the Interreg Grande Region-PULSATEC project.

References

[1] Y.M. Chang, D.K. Mishra, J.M. Ting, Electronic and luminescence properties of sputter-deposited TiO_2 nanostructures, Acta Mater. 61 (2013) 7511–7519, https://doi.org/10.1016/j.actamat.2013.08.066.
[2] K. Kalyanasundaram, A. Grätzel, Applications of functionalized transition metal complexes in photonic and optoelectronic devices, Coord. Chem. Rev. 77 (1998) 347–414, https://doi.org/10.1016/S0010-8545(98)00189-1.
[3] Y. Murakami, E. Kenji, A.Y. Nosaka, Y. Nosaka, Direct detection of OH radicals diffused to the gas phase from the UV-irradiated photocatalytic TiO_2 surfaces by means of laser-induced fluorescence spectroscopy, J. Phys. Chem. B 110 (2006) 16808–16811, https://doi.org/10.1021/jp063293c.
[4] Z. Liu, H. Bai, D. Sun, Facile fabrication of hierarchical porous TiO_2 hollow microspheres with high photocatalytic activity for water purification, Appl. Catal. B Environ. 104 (2011) 234–238, https://doi.org/10.1016/j.apcatb.2011.03.027.
[5] J. Carbajo, A. Bahamonde, M. Faraldos, Photocatalyst performance in wastewater treatment applications: towards the role of TiO_2 properties, Mol. Catal. 434 (2017) 167–174, https://doi.org/10.1016/j.mcat.2017.03.018.
[6] B. O'Regan, M. Grätzel, A low-cost, high-efficiency solar cell based on dye-sensitized colloidal TiO_2 films, Nature 353 (1991) 737–740, https://doi.org/10.1038/353737a0.
[7] O. Carp, C.L. Huisman, A. Reller, Photoinduced reactivity of titanium dioxide, Prog. Solid State Chem. 32 (2004) 33–177, https://doi.org/10.1016/j.progsolidstchem.2004.08.001.
[8] D. Kaczmarek, J. Domaradzki, D. Wojcieszak, E. Prociow, M. Mazur, F. Placido, S. Lapp, Hardness of nanocrystalline TiO_2 thin films, J. Nano Res. 18–19 (2012) 195–200, https://doi.org/10.1109/STYSW.2010.5714178.
[9] V. Stranak, A.-P. Herrendorf, H. Wulff, S. Drache, M. Cada, Z. Hubick, M. Tichy, R. Hippler, Deposition of rutile (TiO_2) with preferred orientation by assisted high power impulse magnetron sputtering, Surf. Coat. Technol. 222 (2013) 112–117, https://doi.org/10.1016/j.surfcoat.2013.02.012.
[10] W. Schönberger, H. Bartzsch, S. Schippel, T. Bachmann, Deposition of rutile TiO_2 films by pulsed and high power pulsed magnetron sputtering, Surf. Coat. Technol. 293 (2016) 16–20, https://doi.org/10.1016/j.surfcoat.2015.12.073.
[11] C. Nouvellon, M. Michiels, J.P. Dauchot, C. Archambeau, F. Laffineur, E. Silberberg, S. Delvaux, S. Konstantinidis, R. Snyders, Deposition of titanium oxide films by reactive high power impulse magnetron sputtering (HiPIMS): influence of the peak current value on the transition from metallic to poisoned regimes, Surf. Coat. Technol. 206 (2012) 3542–3549, https://doi.org/10.1016/j.surfcoat.2012.02.034.
[12] J. Zheng, S. Bao, Y. Guo, P. Jin, TiO_2 films prepared by DC reactive magnetron sputtering at room temperature: phase control and photocatalytic properties, Surf. Coat. Technol. 240 (2014) 293–300, https://doi.org/10.1016/j.surfcoat.2013.12.044.
[13] A. Anders, Tutorial: reactive high-power impulse magnetron sputtering (R-HiPIMS), J. Appl. Phys. 121 (2017), 171101, https://doi.org/10.1063/1.4978350.
[14] A. Anders, J. Andersson, A. Ehiasarian, High power impulse magnetron sputtering: current-voltage-time characteristics indicate the onset of sustained self-sputtering, J. Appl. Phys. 102 (2007), 113303, https://doi.org/10.1063/1.2817812.
[15] J.T. Gudmundsson, N. Brenning, D. Lundin, U. Helmersson, High power impulse magnetron sputtering discharge, J. Vac. Sci. Technol. A 30 (2012), 030801, https://doi.org/10.1116/1.3691832.
[16] V. Kouznetsov, K. Macák, J.M. Schneider, I. Helmersson, I. Petrov, A novel pulsed magnetron sputter technique utilizing very high target power densities, Surf. Coat. Technol. 122 (1999) 290–293, https://doi.org/10.1016/S0257-8972(99)00292-3.
[17] K. Sarakinos, J. Alami, S. Konstantinidis, High power pulsed magnetron sputtering: a review on scientific and engineering state of the art, Surf. Coat. Technol. 204 (2010) 1661–1684, https://doi.org/10.1016/j.surfcoat.2009.11.013.
[18] C.A. Nichols, S.M. Rossnagel, S. Hamaguchi, Ionized physical vapor deposition of cu for high aspect ratio damascene trench fill applications, J. Vac. Sci. Technol. B 14 (1996) 3270–3275, https://doi.org/10.1116/1.588819.
[19] U. Helmersson, L. Martina, B. Johan, A.P. Ehiasarian, J.T. Gudmundsson, Ionized physical vapor deposition (IPVD): a review of technology and applications, Thin Solid Films 513 (2006) 1–24, https://doi.org/10.1016/j.tsf.2006.03.033.
[20] J. Lu, M.J. Kushner, Trench filling by ionized metal physical vapor deposition, J. Vac. Sci. Technol. A 19 (2001) 2652–2663, https://doi.org/10.1116/1.1399318.
[21] F. Magnus, A.S. Ingason, O.B. Sveinsson, S. Olafsson, J.T. Gudmundsson, Morphology of TiN thin films grown on SiO_2 by reactive high-power impulse magnetron sputtering, Thin Solid Films 520 (2011) 1621–1624, https://doi.org/10.1016/j.tsf.2011.07.041.
[22] H. Hajihoseini, M. Kateb, S.P. Ingvarsson, J.T. Gudmundsson, Oblique angle deposition of nickel thin films by high-power impulse magnetron sputtering, J. Nanotechnol. 10 (2019) 1914–1921, https://doi.org/10.3762/bjnano.10.186.
[23] A.P. Ehiasarian, P.Eh. Hovsepian, L. Hultman, U. Helmersson, Comparison of microstructure and mechanical properties of chromium nitride-based coatings deposited by high power impulse magnetron sputtering and by the combined steered cathodic arc/unbalanced magnetron technique, Thin Solid Films 457 (2004) 270–277, https://doi.org/10.1016/j.tsf.2003.11.113.

[24] D. Lundin, J.T. Gudmundsson, N.T. Brenning, M.A. Raadu, T.M. Minea, A study of the oxygen dynamics in a reactive Ar/O_2 high power impulse magnetron sputtering discharge using an ionization region model, J. Appl. Phys. 121 (2017), 171917, https://doi.org/10.1063/1.4977817.
[25] D. Depla, S. Heirwegh, S. Mahieu, J. Haemers, R.De Gryse, Understanding the discharge voltage behavior during reactive sputtering of oxides, J. Appl. Phys. 101 (2007), 013301, https://doi.org/10.1063/1.2404583.
[26] M. Aiempanakit, A. Aijaz, D. Lundin, U. Helmersson, T. Kubart, Understanding the discharge current behavior in reactive high power impulse magnetron sputtering of oxides, J. Appl. Phys. 113 (2013), 133302, https://doi.org/10.1063/1.4799199.
[27] N. Britun, S. Konstantinidis, A. Belosludtsev, T. Silva, R. Snyders, Quantification of the hysteresis and related phenomena in reactive HiPIMS discharges, J. Appl. Phys. 121 (2017), 171905, https://doi.org/10.1063/1.4977819.
[28] T. Kubart, M. Aiempanakit, J. Andersson, T. Nyberg, S. Berg, U. Helmersson, Studies of hysteresis effect in reactive HiPIMS deposition of oxides, Surf. Coat. Technol. 205 (2011) 5303–5306, https://doi.org/10.1016/j.surfcoat.2011.01.019.
[29] V. Sittinger, F. Ruske, W. Werner, C. Jacobs, B. Szyszka, D.J. Christie, High power pulsed magnetron sputtering of transparent conducting oxides, Thin Solid Films 516 (2008) 5847–5859, https://doi.org/10.1016/j.tsf.2007.10.031.
[30] F. Ruske, A. Pflug, V. Sittinger, W. Werner, B. Szyszka, D.J. Christie, Reactive deposition of aluminium-doped zinc oxide thin films using high power pulsed magnetron sputtering, Thin Solid Films 516 (2008) 4472–4477, https://doi.org/10.1016/j.tsf.2007.06.019.
[31] V. Tiron, L. Sirghi, Tuning the band gap and nitrogen content of ZnO_xN_y thin films deposited by reactive HiPIMS, Surf. Coat. Technol. 282 (2015) 103–106, https://doi.org/10.1016/j.surfcoat.2015.10.017.
[32] T. Shimizu, M. Villamayor, D. Lundin, U. Helmersson, Process stabilization by peak current regulation in reactive high-power impulse magnetron sputtering of hafnium nitride, J. Appl. Phys. 49 (2016), https://doi.org/10.1088/0022-3727/49/6/06520.
[33] J. Vlček, J. Rezek, J. Houška, R. Čerstvý, R. Bugyi, Process stabilization and a significant enhancement of the deposition rate in reactive high-power impulse magnetron sputtering of ZrO_2 and Ta_2O_5 films, Surf. Coat. Technol. 236 (2013) 550–556, https://doi.org/10.1016/j.surfcoat.2013.10.052.
[34] J. Vlcek, J. Rezek, J. Houska, T. Kozak, J. Kohout, Benefits of the controlled reactive high-power impulse magnetron sputtering of stoichiometric ZrO_2 films, Vac 114 (2015) 131–141, https://doi.org/10.1016/j.vacuum.2014.12.004.
[35] M. Audronis, V. Bellido-Gonzalez, B. Daniel, Control of reactive high power impulse magnetron sputtering processes, Surf. Coat. Technol. 204 (2010) 2159–2216, https://doi.org/10.1016/j.surfcoat.2009.11.040.
[36] W.-Y. Wu, B.-H. Hsiao, P.-H. Chen, W.-C. Chen, C.-T. Ho, C.-L. Chang, CrNx films prepared using feedback-controlled high power impulse magnetron sputter deposition, J. Vac. Sci. Technol. A 32 (2014) 02B115, https://doi.org/10.1116/1.4862147.
[37] J. Xiurong, F.-C. Yang, J.-W. Lee, C.-L. Chang, Effect of an optical emission spectrometer feedback-controlled method on the characterizations of nc-TiC/a-C:H coated by high power impulse magnetron sputtering, Diam. Relat. Mat. 73 (2017) 19–24, https://doi.org/10.1016/j.diamond.2016.11.007.
[38] C.-L. Chang, F.-C. Yang, Synthesis and characteristics of nc-WC/a-C:H thin films deposited via a reactive HIPIMS process using optical emission spectrometry feedback control, Surf. Coat. Technol. 350 (2018) 1120–1127, https://doi.org/10.1016/j.surfcoat.2018.02.006.
[39] A.D. Pajdarova, J. Vlcek, J. Rezek, Optical emission spectroscopy during the deposition of zirconium dioxide films by controlled reactive high-power impulse magnetron sputtering, J. Appl. Phys. 121 (2017), https://doi.org/10.1063/1.4977822.
[40] S. Vargas, D.S. Galeano-Osorio, C.E. Castano, Controlling preferential growth of chromium – nitrogen R-HiPIMS and R-DCMS films by substrate magnetic biasing, Appl. Surf. Sci. 569 (2021), https://doi.org/10.1016/j.apsusc.2021.151113.
[41] V. Tiron, I.-L. Velicu, I. Mihăilă, G. Popa, Deposition rate enhancement in HiPIMS through the control of magnetic field and pulse configuration, Surf. Coat. Technol. 337 (2018) 484–491, https://doi.org/10.1016/j.surfcoat.2018.01.065.
[42] J.T. Gudmundsson, D. Lundin, N. Brenning, M.A. Raadu, C. Huo, T.M. Minea, An ionization region model of the reactive Ar/O_2 high power impulse magnetron sputtering discharge, Plasma Source Technol. 25 (2016), 065004, https://doi.org/10.1088/0963-0252/25/6/065004.
[43] A.E.L. Farsy, J. Ledig, M. Desecures, J. Bougdira, L. de Poucques, Characterization of transport of titanium neutral atoms sputtered in Ar and Ar/N_2 HIPIMS discharges, Plasma Sources Sci. Technol. 28 (2019), 035005, https://doi.org/10.1088/1361-6595/ab022b.
[44] G.-S. Chen, C.-C. Lee, H. Niu, W. Huang, R. Jann, T. Schütte, Sputter deposition of titanium monoxide and dioxide thin films with controlled properties using optical emission spectroscopy, Thin Solid Films 516 (2008) 8473–8478, https://doi.org/10.1016/j.tsf.2008.04.093.